

# An Architecture for High Data Rate Very Low Frequency Communication

Arun Kumar\* and Rajendar Bahl

Indian Institute of Technology - Delhi, New Delhi - 110 016

\*E-mail: arunkm@care.iitd.ac.in

## ABSTRACT

Very low frequency (VLF) communication is used for long range shore-to-ship broadcasting applications. This paper proposes an architecture for high data rate VLF communication using Gaussian minimum shift keying (GMSK) modulation and low delay parity check (LDPC) channel coding. Non-data aided techniques are designed and used for carrier phase synchronization, symbol timing recovery, and LDPC code frame synchronization. These require the estimation of the operative  $E_b/N_0$  for which a kurtosis based algorithm is used. Also, a method for modeling the probability density function of the received signal under the bit condition is presented in this regard. The modeling of atmospheric radio noise (ARN) that corrupts VLF signals is described and an algorithm for signal enhancement in the presence of ARN is given. The BER performance of the communication system is evaluated for bit rates of 400 bps, 600 bps, and 800 bps for communication bandwidth of ~200 Hz.

**Keywords:** Communication systems, VLF Communication, GMSK modulation, LDPC codes, atmospheric radio noise

## 1. INTRODUCTION

The very low frequency (VLF) band of 3 kHz to 30 kHz is used for strategic long range communication from shore to ship, in particular, near-surface submarines. The navies of various countries place a lot of importance to the use of VLF band for broadcasting information to submarines. It is thus a simplex mode of communication. The allocated bandwidth is typically limited to the order of 200 Hz. Because of the limited bandwidth, the message source is only text or data and not voice. Classically, frequency shift keying (FSK) and minimum shift keying (MSK) have been used as the modulation techniques for VLF communication with data rates of 50-200 bps. In this paper, authors report the design of an architecture for high data rate VLF communication between 400-800 bps. The key elements of the high data rate communication system are Gaussian minimum shift keying (GMSK) modulation and low delay parity check (LDPC) channel coding. The architecture is completely non-data aided. Thus, carrier phase synchronization, timing recovery, and LDPC frame synchronization algorithms use properties of the signal rather than preamble or header data to perform the respective tasks.

The block level description of the communication transmitter and receiver is given in Fig. 1. The transmitter encodes the non-return to zero (NRZ) source data using LDPC codes. The coded data is modulated using GMSK and is transmitted. The output of the source block is assumed to be source encoded.

The receiver chain begins with a pass-band analog antenna filter which limits the signal and noise in the band of the signal. The signal enhancement block filters the signal to reduce the atmospheric radio noise (ARN) component. The output is passed through an IF filter with a bandwidth

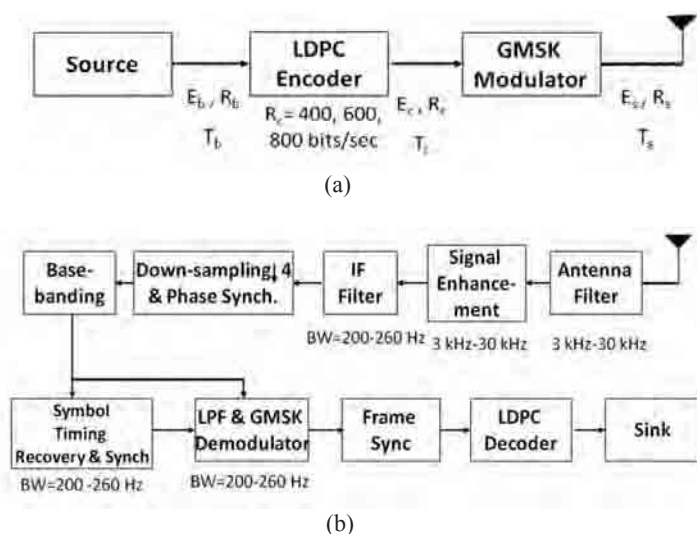


**Figure 1. Block diagram architecture of (a) VLF transmitter, and (b) VLF receiver.**

of 200-260 Hz depending upon the signal bandwidth. The output of this filter is down-sampled and subjected to carrier phase synchronization for base-banding the signal in the next block. The band-band signal is low pass filtered and symbol timing recovery and synchronization is performed next. The base-band signal is low pass filtered and GMSK demodulation is performed using alternating in-phase quadrature (AIQ) coherent demodulator. The LDPC frame synchronization block determines and tracks the start of the frame. LDPC decoding is done on a frame-by-frame basis. The output of the LDPC decoder is presented for source decoding and extraction of

the NRZ data. For each block, several competing alternatives were considered and simulated for checking their suitability in the proposed architecture. For high data rates, two choices are available in GMSK modulation viz. binary and M-ary GMSK. The preference of binary GMSK over 4-ary GMSK for 600 bps and 800 bps rates is explained. Furthermore, the non-data aided synchronization tasks required the use of novel techniques that are described.

## 2. GAUSSIAN MINIMUM SHIFT KEYING MODULATION AND DEMODULATION

Gaussian minimum shift keying is commonly used for modulation in mobile and wireless communication systems including GSM because of its various advantages<sup>1-4</sup>. The GMSK is a spectrally efficient digital modulation scheme. It is derived from generic MSK, which is a binary digital FM scheme with a modulation index of 0.5 and has good properties of constant envelope, relatively narrow bandwidth and coherent detection capability. However, MSK which is classically used for VLF communication does not satisfy the typically severe requirements with respect to out-of-band radiation that is an important consideration in VLF communication. A pre-modulation low-pass filter can be used to alter the power spectrum in MSK while keeping the constant envelope property. When a Gaussian lowpass pre-filter is used, the modulation scheme is called GMSK. Compared to MSK, the Gaussian pre-filter helps in suppressing the high-frequency components and reducing excessive instantaneous frequency deviation.

The error probability of GMSK is greater than that of MSK due to the trade-off between power and bandwidth efficiency. GMSK achieves better bandwidth efficiency than MSK at the expense of power efficiency so there is ISI, which is a bandwidth limiting factor. The main characteristic of GMSK modulation is the product of -3 dB bandwidth of the pre-modulation Gaussian low pass filter  $B_{-3dB}$ , and the symbol duration  $T$ , and is called the BT product. The pulse shape of the output bit stream is dependent on the BT product. A lower BT product implies lowering the amplitude and increasing the pulse width which causes an increase in the inter-symbol interference (ISI). It may be noted that GMSK with  $BT = \infty$  is equivalent to MSK. While increasing the ISI allows the spectrum to be more compact, it also makes demodulation more difficult. A common way to implement the GMSK modulator is the quadrature baseband method which can maintain the modulation index exactly at 0.5 for the binary case<sup>5</sup>. For M-ary GMSK modulation, the input data has M-levels and the modulation index is typically chosen as  $1/M$ <sup>6</sup>.

Authors consider 3 transmission bit rates of 400 bps, 600 bps, and 800 bps for a theoretical 2-sided bandwidth of 200 Hz for each case. For binary GMSK, and one-sided -3 dB bandwidth of 100 Hz, the respective BT products used are 0.25, 0.167 and 0.125 respectively for modulation index  $h = 0.5$ . Table 1 gives the measured -3 dB bandwidth for the 3 cases. The measurement is done by averaging the spectrum over about 6000 frames each containing about 2000 bits. An alternative method for higher data rates is to use M-ary GMSK. For example, for 600 bps and 800 bps, one can use  $M = 4$  which results in symbol rates of 300 baud and 400 baud respectively. The measured-3 dB bandwidth for 4-ary GMSK for these two rates is also given in Table 1. It can be seen that the binary GMSK for the 600 bps and 800 bps data rates is spectrally more compact than for the 4-ary case. The BER performance of binary and 4-ary GMSK was compared for  $BT = 0.167$  and 0.33 respectively which would result in the same data rates for the 2 cases<sup>6,7</sup>. Fig. 2 shows these BER plots. It can be inferred that the binary case shows slightly better performance than the 4-ary case. In view of the above two advantages of binary GMSK over 4-ary GMSK, the binary GMSK modulation scheme has been chosen for all the 3 data rates.

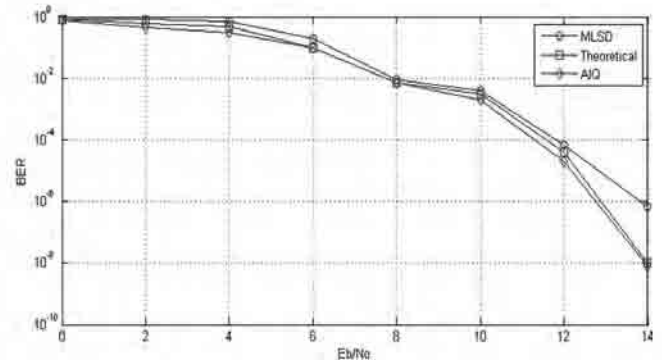


Figure 2. BER vs  $E_b/N_0$  (in dB) for uncoded binary GMSK from simulation compared with uncoded 4-ary GMSK<sup>23</sup>.

There are several methods for GMSK demodulation spanning both non-coherent and coherent techniques. While coherent processing techniques are complex, they are usually preferred due to the better error performance compared to non-coherent processing techniques. Coherent demodulation requires knowledge of the reference phase or the exact phase needs to be recovered, thus requiring local oscillators, phase-lock loops, and carrier recovery circuits which add to the receiver complexity. The non-coherent demodulation techniques for GMSK include:

Table 1. Specifications of binary and 4-ary GMSK modulated signal for various data rates.

M	Modulation index ( $h$ )	BT	Symbol rate ( $R_s$ )	Bit rate ( $R_b$ )	Measured -3dB bandwidth (Hz)
2	0.5	0.25	400	400	160
2	0.5	0.167	600	600	200
2	0.5	0.125	800	800	240
4	0.25	0.33	300	600	220
4	0.25	0.25	400	800	260

- Limiter discriminator receiver<sup>8</sup>, and
- Differential demodulator with and without decision feedback<sup>9</sup>.

The coherent demodulation techniques include:

- Alternating in-phase quadrature (AIQ) demodulator<sup>10</sup>,
- Differential coherent detection via the Viterbi algorithm<sup>11</sup>,
- Linear receiver<sup>11</sup>, and
- Differential coherent detection via the Viterbi algorithm with phase estimation<sup>12</sup>.

The common approach in the above coherent receivers is to consider the GMSK modulated signal as a class of binary continuous phase modulated (CPM) signal and use differential coherent detection via a maximum-likelihood sequence detector based on the Viterbi algorithm. The binary CPM signal is approximated by a sum of PAM signals. Laurent showed that the baseband CPM signal can be written as a sum of  $2^{L-1}$  PAM signals, where in the case of GMSK, L is the number of symbols over which the impulse response of the Gaussian pre-filter extends<sup>13</sup>. The complexity of the Viterbi algorithm (VA) is proportional to the number of decoder states. This is because the transmitted signal is composed of a relatively large number of PAM components. The complexity is often reduced by basing the decision on approximate signals composed of a smaller number of PAM components.

The AIQ demodulation method is a low complexity technique with nearly optimal decoding performance. It uses the principal Laurent PAM filter only that outputs the maximum energy component, and thereby avoids the use of the Viterbi based decoder. The outputs of the in-phase and quadrature-phase channels sampled at the symbol rate provide the alternate symbol information which can be used as soft information in the subsequent block for LDPC decoding, or can be thresholded for hard decision on the bits<sup>10</sup>. As discussed in the earlier section, both soft and hard decisions will be required for LDPC decoding.

Figure 3 compares the BER performance of a maximum likelihood sequence detector (MLSD) demodulator with the AIQ demodulator through simulations based on the transmission of  $10^{10}$  coded bits. It can be inferred that the AIQ demodulator provides consistently better BER performance with an advantage of about 1 dB or more over the  $E_b/N_0$  range

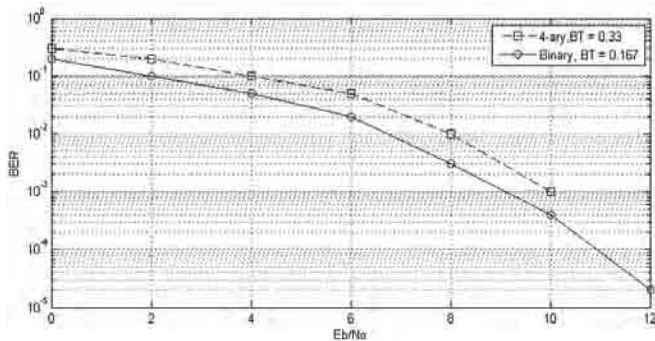


**Figure 3. BER vs  $E_b/N_0$  (in dB) of MLSD and AIQ demodulators for uncoded GMSK obtained from simulation. For the AIQ demodulator, the theoretical plot is also provided for reference.**

of 0 to 14 dB that was tested. For reference, the theoretical BER plot is also obtained from  $P_e = Q \{ (2a E_b/N_0)^{1/2} \}$ , where  $Q\{.\}$  is the Q-function,  $a = 0.68$  for  $BT = 0.25$ <sup>14</sup>.

### 3. CARRIER PHASE SYNCHRONIZATION AND SYMBOL TIMING RECOVERY

A coherent demodulator requires carrier frequency and phase recovery for base-banding. If the frequency drift is very small such that its explicit recovery can be neglected, then the recovery of phase becomes the major requirement. Costas loop is one such non-data-aided method that can be used in principle for GMSK signals<sup>15</sup>. In VLF communication, the frequency drift can be considered to be very small and therefore authors are concerned primarily with the requirement of carrier phase synchronization. The message bit information in the GMSK signal is contained in its phase. The channel may introduce phase error in the received signal leading to erroneous demodulation and message extraction. This stipulates the need for exact carrier phase recovery for base-banding.

Both data-aided and non-data aided techniques can be considered. Data aided techniques have the potential to perform relatively well in low SNR conditions, but at the cost of reduced throughput. In one data-aided technique, a preamble is inserted explicitly for this purpose. For example, a linear up-chirp or linear down-chirp or up-down chirp for the duration of several symbols can be sent along with the GMSK signal, and at the receiver, the received signal can be match filtered with the known preamble (without phase). The phase lag can be determined from the offset from the centre. In the non-data aided category, one simple method is that of carrier burst, in which the carrier waveform of several symbols duration and relatively small amplitude is added periodically to the GMSK signal and transmitted. At the receiver, the carrier is extracted by auto-correlating the received signal with the known carrier. The phase lag is determined from the offset from the centre.

The non-data aided carrier phase synchronization technique considered in this work is the maximum *a posteriori* probability one-amplitude modulated pulse method also referred to as the MAP one-AMP method<sup>16</sup>. The synchronizer is based on the Laurent decomposition of the received signal. The received signal is multiplied with the locally generated carrier with some phase error. The base banded in-phase and quadrature-phase signals are matched filtered considering only one Laurent PAM filter for the one-AMP scheme. The matched filter outputs are sampled and their tanh function are taken. These respective terms are multiplied and subtracted. The output is fed to a digital loop filter which is used in order to pass only the D.C. component (error signal) of the incoming signal. This error signal is the input for the VCO, which generates the local carrier at the receiver.

The purpose of the symbol timing recovery loop is to obtain symbol synchronization by altering the sampling phase as required to sample the symbols at the peaks. This phase adjustment may be performed either by actually altering the sampling instants (choosing samples before or after the center sample of the pulse) or by altering the phase of the matched filter impulse response itself. Depending upon whether the timing is early or late, we may use a phase delayed or advanced

version of the matched filter impulse response to match the timing offset so that the center sample of the pulse corresponds to the highest SNR point.

One method for timing recovery is the frequency discriminator which is a differentiator device. It finds the zero-crossing points of the transmitted signal (GMSK). The separation between the zero-crossing points is found which is used for obtaining the sampling instant for the symbols. The draw-back of this approach is the requirement of very high sampling frequency so that the values of zero-crossing points of the GMSK signal are accurately found. Hence, this method has not been used.

Another method for symbol timing recovery is called the squaring algorithm<sup>17</sup>. The timing information can be obtained by viewing the GMSK signal as a combination of two orthogonal linear modulations each with symbol rate  $1/2T$  and staggered with a time  $T$ . Timing delays are estimated separately in the I and Q channels and the two estimates are combined to give the timing delay estimate for the GMSK signal. This method has been used for the purpose of symbol timing recovery.

The squaring algorithm has been implemented in the recovery of symbol timing and synchronization at the sample level for symbol detection. The carrier phase estimation algorithm presents a phase ambiguity of 45 degrees. This is removed by considering two parallel channels in the symbol timing recovery block with two phase estimates separated by 45 degrees. A frame of symbols is divided into 10 equal length sub-frames, from which 10 estimates of the timing information are obtained in each of the 2 channels. The variance of the timing information in the 2 channels is computed. The channel with lower variance is used as the correct phase and the other channel with 45 degree offset in the carrier phase is rejected. The algorithm flow is shown in Fig. 4. This method requires buffering of the received data for the duration of one frame which may span up to 3s - 5s. Since VLF communication is generally simplex, this delay is not a practical limitation. Figure 5 shows the performance of the squaring algorithm in symbol timing recovery through plots of the RMS timing error in number of samples vs  $E_b/N_0$  for various number of data bits used in estimation. The initial carrier phase offset is assumed to be the worst case at 22.5 degrees.

#### 4. LDPC CODING AND FRAME SYNCHRONIZATION

Low delay parity check (LDPC) block codes, discovered by Gallager in 1962, were not used till about 1995 because of the high computational requirements of the decoder<sup>18-20</sup>. A low density parity check code is a block code which has a very sparse parity check matrix (the generator may or may not be sparse). These are also called Gallager codes. LDPC codes have performance similar to that of turbo codes that have found wide use in the last two decades, though iterative decoding algorithms are easy to implement, due to the lower per-iteration complexity than that of turbo codes<sup>21,22</sup>. Following are the important features of LDPC codes which make them suitable for use as error control codes in the present architecture:

- Random construction which gives the capability of performing close to Shannon's limit.

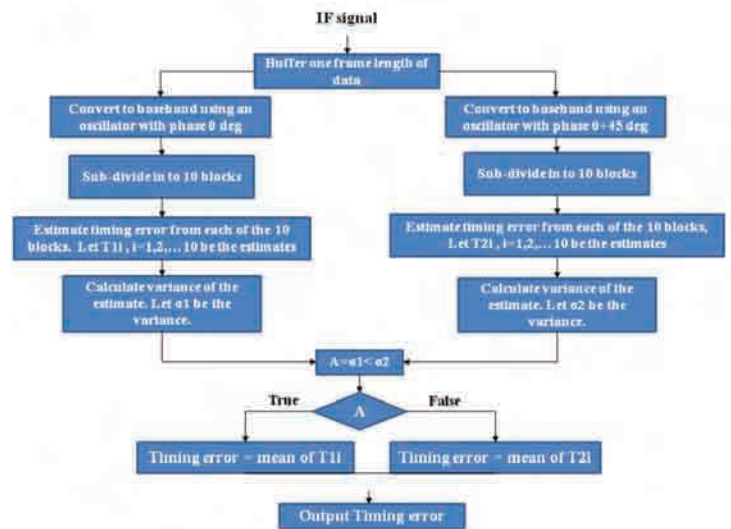


Figure 4. Algorithm flow for the estimation of unambiguous carrier phase from symbol timing variance computation.

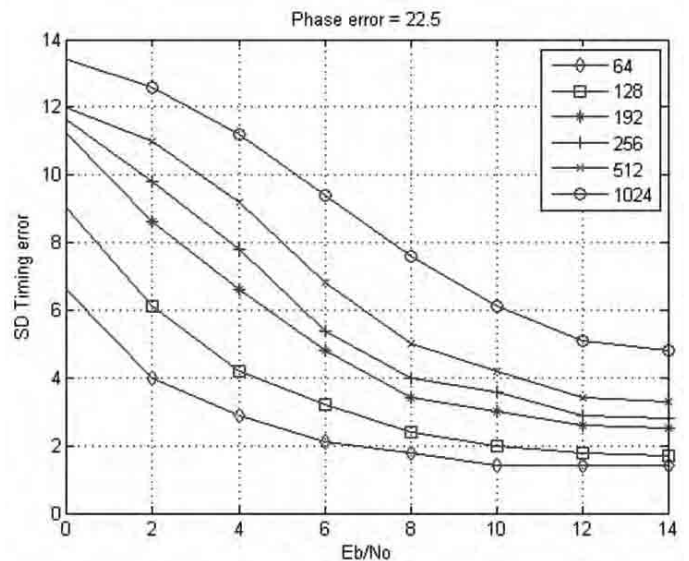


Figure 5. RMS symbol timing error in number of samples vs.  $E_b/N_0$  for various number of bits used in estimation. The initial carrier phase offset is assumed to be 22.5 degrees.

- Minimum distance of code which increases linearly with code length keeping the column weight constant. This offers two advantages viz., sparser matrices which lower the decoding complexity and longer codes for better error correcting capability.
- LDPC codes perform better than turbo codes for higher code rates (greater than 0.5), though they perform poorly compared to turbo codes at lower code rates.
- LDPC decoders also offer high degree of parallelism. Despite several potential advantages of LDPC codes, in burst error conditions, Reed Solomon codes perform better. However, such a situation is not typically encountered in a VLF channel and hence it justifies the use of LDPC codes for VLF communication. LDPC codes can be classified into the following categories

based on the structure of the parity check matrix and the code properties:

- **Block and Convolutional LDPC Codes:** LDPC block codes (LDPC-BC) are block codes with sparse parity check matrix that operate on a discrete block of bits<sup>18,23</sup>, while LDPC convolutional codes (LDPC-CC) operate on continuous bit stream<sup>24-6</sup>. For comparable error performance, the former requires a very large block length compared to the constraint length of the latter. A detailed comparison of the two types can be found in the literature<sup>27</sup>.
- **Regular and Irregular LDPC Codes:** The LDPC codes suggested by Gallager in 1962 had parity check matrix with uniform row and column weights. Later on, generalization of Gallager's codes by a number of researchers led to the development of parity check matrices with non-uniform row and column weights<sup>28,29</sup>. Consequently, the former class was named regular LDPC codes and the latter, irregular LDPC codes. Irregular codes demonstrate far superior error performance than regular ones under similar circumstances. The decoding and encoding algorithm remains exactly the same for both.
- **Non-Cyclic, Cyclic, and Quasi-Cyclic LDPC Codes:** LDPC codes can be constructed to be in any of the above three forms. Non-cyclic codes are those in which codewords are not cyclic shifts of each other. Cyclic codes are those in which a word formed by a cyclic left or right shift by one position of a codeword is also a codeword. Quasi-cyclic codes are those in which cyclic left or right shift of a codeword by  $p$  positions results in another codeword. Cyclic code is a particular case of quasi-cyclic code when  $p=1$ . Cyclic and quasi-cyclic forms present certain order of simplicity in encoding and decoding<sup>18, 23</sup>.

The MacKay and Neal construction method has been used to generate the LDPC block codes. Both regular and irregular LDPC block codes could be generated using this method. The degree distribution pairs have been chosen for irregular LDPC code construction<sup>23</sup>. The generation of LDPC cyclic codes has also been done from LDPC block codes itself.

The frame synchronization problem involves determining the start of each frame of data streaming in continuously. It is usually achieved by concatenating a known synchronization word or a signal at the beginning of a frame. At the receiver, the data is correlated with a delayed replica of the concatenated sync signal and the delay at which a threshold is overshoot, a frame start event is declared. The paucity of bandwidth in the VLF band renders such pilot signal based frame synchronization methods useless and motivates the use of pilotless schemes.

The structural properties of LDPC codes have been exploited for pilotless frame synchronization and found to provide very low frame error rate (FER) even at low values of  $E_b/N_0$ <sup>30</sup>. The maximum likelihood method is proposed to be used in the receiver architecture for frame synchronization prior to LDPC decoding in the VLF modem. It involves deciding the true frame offset as the one which maximizes the number of satisfied constraints. The number of satisfied constraints varies as the window slides across the decoded hard bits at the output of the demodulator. At the correct frame match, the number of satisfied constraints increases significantly above the

neighboring positions. This can be used to detect the start of frame. Figure 6 gives a plot of mean offset error in number of bits vs.  $E_b/N_0$  for LDPC coded GMSK frame synchronization. It can be seen that the frame offset error is zero for  $E_b/N_0$  of 5 dB or greater for code rates of 1/2 and 4/5.

For LDPC decoding, both hard and soft decoding algorithms are available for decoding LDPC codes along with their several variants<sup>18,19,23</sup>. The bit flipping method belongs to the first category while the iterative log likelihood decoding algorithm belongs to the second category. The latter provides significantly better coding gain even at low values of  $E_b/N_0$ .

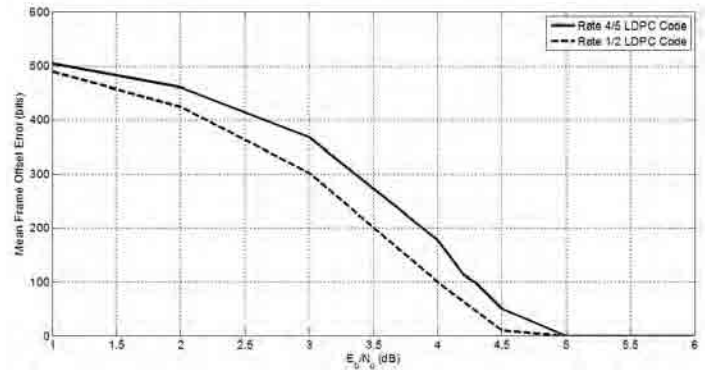


**Figure 6. Mean offset error in number of bits vs.  $E_b/N_0$  for LDPC coded GMSK frame synchronization.**

However, as explained in the previous paragraph, it is necessary to also do hard decoding for pilotless frame synchronization purpose. The bit flipping algorithm is a hard-decision message passing algorithm for LDPC codes<sup>18,23</sup>. Both the hard bit flipping and soft log likelihood decoding algorithms were implemented and used for performance evaluation of LDPC codes constructed using MacKay and Neal method.

The soft decoder requires the log likelihood ratios of the bit a posteriori probabilities corresponding to the transmitted bit sequence. It is straightforward to find the likelihood ratios for BPSK, since, the soft bits from the matched filter follow the Gaussian distribution<sup>18</sup>. Similar results for GMSK with AIQ detector are not found. Thus, it is necessary to model the distribution of the matched filter outputs conditioned on the transmitted bit so as to compute the likelihood ratios and proceed with LDPC decoding.

To estimate the probability density model, the histograms of the AIQ detector outputs are obtained. The density of soft bits is observed to be Gaussian for low noise levels. However, for medium and high noise levels, the distribution of soft bits for every '1' transmitted demonstrated a positive skewness and vice versa for every '0' transmitted. Thus, the distribution is modeled using a Gaussian mixture model (GMM). While fitting the empirical distribution of AIQ outputs, 1 to 6 mixture components were used. It is found that no less than four components are required to provide a good fit for all possible values the soft bit can take. Also, using more than four components did not provide any better fit. Thus, 4 mixture component GMM is proposed for modeling the a posteriori probability density of the soft bits.

The GMM probability density function (pdf) parameters for the two binary decoded bit cases are generated from

receiver data for different known  $E_b/N_0$  values and stored as a look-up table and used by the LDPC decoder. Thus, to use the look-up table to furnish the parameters to the LDPC decoder correctly, an  $E_b/N_0$  estimation algorithm is also required which is discussed next.

In the following authors consider the non-data aided SNR estimation method. An  $E_b/N_0$  or SNR estimation technique is required to generate *a posteriori* probabilities of bits conditioned on the received signal to input to the LDPC decoder. A kurtosis based algorithm is proposed for the computation of SNR over AWGN channel<sup>31</sup>. Let:

$$y(t) = x(t) + n(t) \quad (1)$$

where,  $y(t)$ ,  $x(t)$ , and  $n(t)$  are the received signal, transmitted signal, and additive noise respectively. The normalized SNR, given by  $S$  is calculated by solving the equation,

$$K_y = S^2 K_x + (1 - S)^2 K_n \quad (2)$$

where  $K_y$ ,  $K_x$  and  $K_n$  denotes the excess kurtosis of the received signal, the transmitted signal, and channel noise respectively. The SNR is then computed as,

$$\text{SNR (dB)} = 10 \log_{10} (S / (1-S)) \quad (3)$$

The excess kurtosis of the transmitted signal is fixed for a particular modulation scheme and is known *a priori*. For example,  $K_x = -1.5$  for BPSK and GMSK. The excess kurtosis of Gaussian noise is zero. Hence, Eqns (2) and (3) give the estimate of SNR and therefore,  $E_b/N_0$  assuming AWGN. After the signal enhancement that removes impulsive noise component of ARN as discussed in the next section, the remaining noise component can be approximated as AWGN, and the above method can be applied to estimate the SNR and  $E_b/N_0$ .

## 5. ATMOSPHERIC RADIO NOISE MODELING AND SIGNAL ENHANCEMENT

The VLF communication is in the band of 3-30 KHz which is strongly affected by atmospheric noise<sup>32-34</sup>. The models for the atmospheric radio noise (ARN) can be broadly classified as the empirical models, and the statistical-physical models<sup>35-39</sup>. The empirical models are based on intuitive reasoning and/or fitting the data to mathematical functions, such as the Hall model, the Field and Lewenstein model, and the  $\alpha$ -stable model. On the other hand, the statistical-physical models start with assumptions on noise source distributions and the propagation of noise impulses to the receiver. The empirical models are mathematically more tractable than the statistical-physical models, but their parameters are often unrelated to the physical processes that create the noise. Some examples of the statistical-physical models are the Middleton class A and B noise models and the clustering-Poisson model.

The atmospheric noise is non-Gaussian (impulsive) in nature and has heavy-tailed distribution. The impulses are caused by atmospheric events, mainly lightning strokes that create electromagnetic emissions known as sferics. 'Sferics,' which is the short form for 'radio atmospherics' are impulsive signals generated by lightning strokes that travel in the Earth-ionosphere wave-guide. These impulsive signals (a few ms duration) propagate for thousands of kilometers. The amount of sferic activity in a given noise sample depends on the worldwide distribution of lightning relative to the receiver

location, with nearby thunderstorms contributing a great deal and distant storms contributing less. The study of such noise waveforms show that these impulses tend to cluster in groups, indicating an underlying clustering process related to the physical characteristics of the lightning mechanism<sup>40</sup>. Also, since the ARN is highly impulsive, it is better modeled as  $\alpha$ -stable distributed.

The clustering Poisson model is based on several previously known statistical-physical models, but in addition takes into account the clustering of sferic impulses<sup>40,41</sup>. The atmospheric noise is viewed as a superposition of Gaussian noise and distinct impulses. The Gaussian component is the background noise, which results from the superposition of numerous low-level sources, including distinct sferics. Lightning from relatively nearby thunderstorms causes the impulses. Signal enhancement algorithms were tested using ARN based on the clustering Poisson model.

The placement of the median filter and the Wiener filter for signal enhancement are shown in Fig. 7(a). The median filter is placed after the receiving antenna (modeled by the band-pass filter with passband ranging from 3 kHz to 30 kHz) and the A-D converter operating at a high sampling rate to avoid spreading of the noise impulses in the time domain due to further down-sampling. After suppression of noise impulses by the median filter, the signal is passed through a band-pass filter with bandwidth 200 Hz and centered about the carrier frequency. The signal is down-sampled and passed through the Wiener filter to suppress the Gaussian-distributed background noise. The estimate of noise variance required by the Wiener filter is based on the estimation of kurtosis of the signal over one frame of data (as described in the previous section) that is an input to the Wiener filter.

The length of the window over which the median value is calculated for each time sample is determined as depicted in Fig. 7(b). The cumulative density function (CDF) for the absolute value of the noisy signal at the input of the median filter is determined. The amplitudes of the noise pulses are much higher as compared to that of the sum of the signal and the background noise. Since the occurrence of the amplitude values corresponding noise pulses is relatively much sparse on the time axis, the amplitude value for which the CDF exceeds 0.995 is taken as the threshold value, shown by the symbol 'th' in Fig. 7(b). Thus, whenever the absolute amplitude of the signal is greater than the threshold value, it indicates the presence of the noise pulse. The location of the noise pulses so detected and their duration, i.e. the duration over which the absolute amplitude of the signal continuously stays above the threshold value, is found over the complete length of the signal which is one frame in this case. The length of the median filter is taken as three times the maximum duration of the noise pulse in the frame. The median filter is applied only on the detected noise pulses. The performance of the signal enhancement method in the presence of ARN is described in the next section.

## 6. INTEGRATED RECEIVER PERFORMANCE

The integrated receiver requires the initialization of the synchronization blocks and identification of the LDPC frame for proper decoding. For this purpose, three frames of data

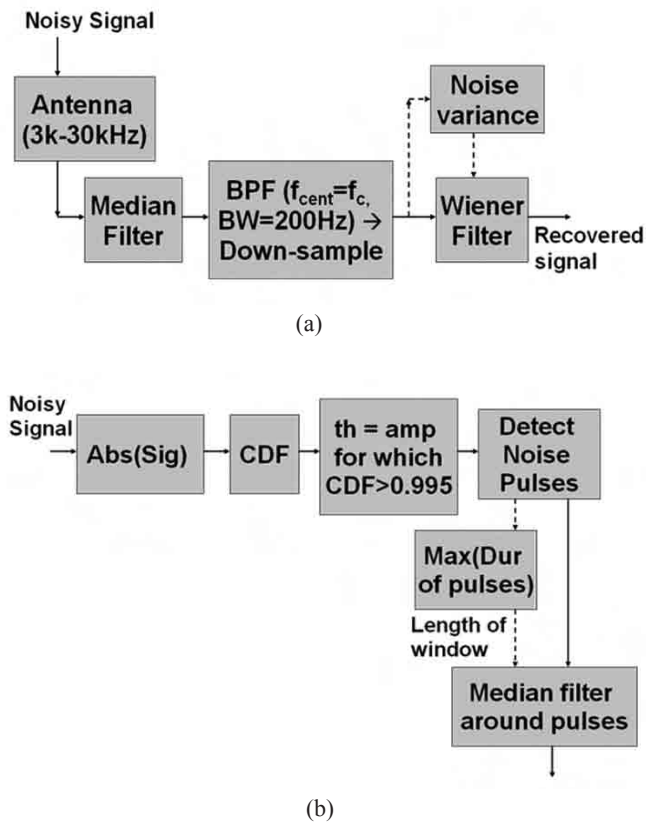
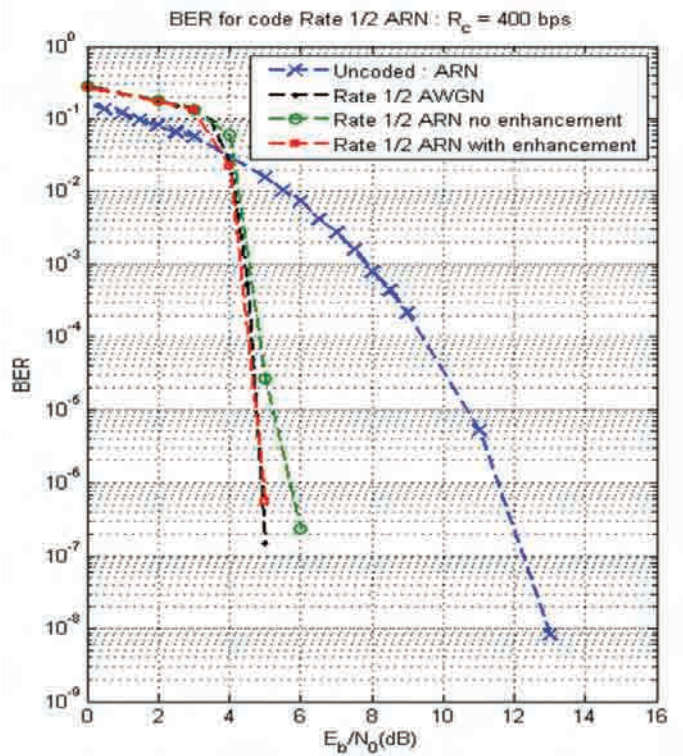
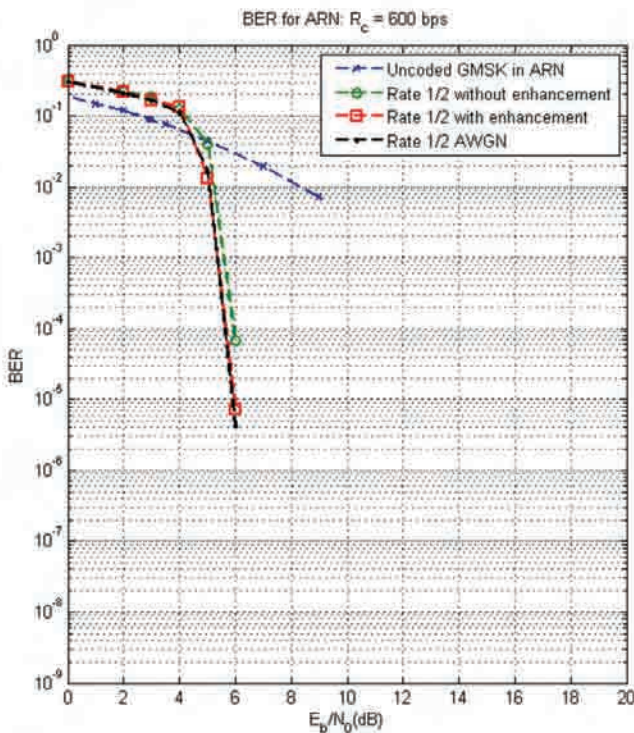


Figure 7. (a) Signal enhancement method in the presence of atmospheric radio noise in the received signal, and (b) Detailed flow of the median filter block.

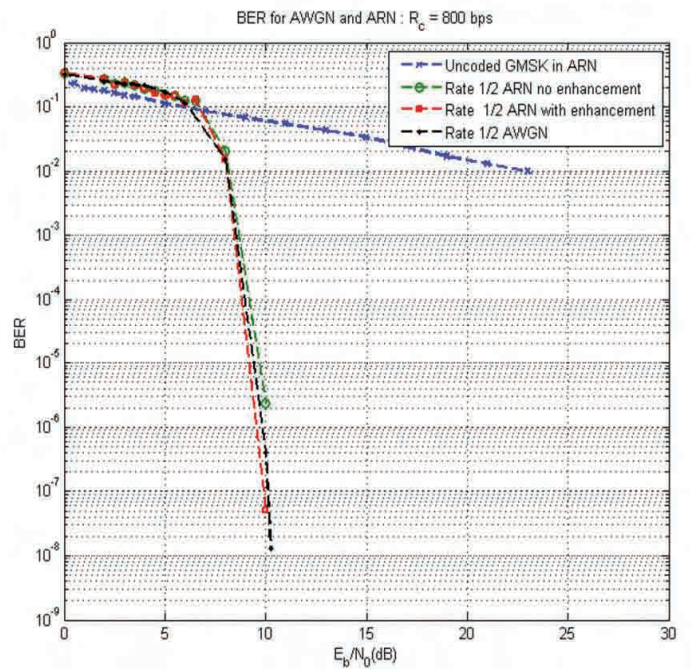
are buffered initially from the arbitrary starting instant. An arbitrary local oscillator phase is initialized for the carrier frequency. The symbol timing recovery is done with the available carrier phase. This symbol timing information is used to perform carrier phase synchronization over the buffered data.



(a)



(b)



(c)

Figure 8. BER performance of LDPC coded GSMK communication system for (a) 400 bps, (b) 600 bps, (c) 800 bps coded data rates. Plots in each graph show performances for (i) unencoded GSMK in ARN, (ii) LDPC coded GSMK in AWGN, (iii) LDPC coded GSMK in ARN without signal enhancement, (iv) LDPC coded GSMK in ARN with signal enhancement.

The two steps are repeated 5-10 times to improve the carrier phase synchronization and symbol timing synchronization iteratively. This data is used to perform frame synchronization. From the identified frame starting bit, the frames are decoded successively thereafter.

The BER performance of LDPC coded GMSK communication system for coded bit rates of 400 bps, 600 bps, and 800 bps is shown in Figs. 8(a) - 8(c). The simulation study is based on the decoding of  $10^9$  bits of data. The plots in each graph show the performances for

- uncoded GMSK in ARN,
- LDPC coded GMSK in AWGN,
- LDPC coded GMSK in ARN without signal enhancement,
- LDPC coded GMSK in ARN with signal enhancement.

The  $E_b/N_0$  used for the characterization of receiver performance in ARN is derived as follows. First, the AWGN corresponding to the  $E_b/N_0$  is obtained and added to the signal. Thereafter, the clustering Poisson process realization corresponding to the impulsive noise component of ARN is generated and added. Thus, for comparing the BER plots obtained with AWGN and ARN, it may be noted that at a given  $E_b/N_0$ , the AWGN variance is the same in both cases, whereas the ARN contains extra impulsive noise that is not considered in the  $E_b/N_0$  values. In other words, for a given  $E_b/N_0$ , ARN has greater variance compared to AWGN.

It can be seen from the graphs that, (i) the BER reduces below  $10^{-6}$  at 5 dB and 10 dB  $E_b/N_0$  for 400 and 800 bps rates respectively and below  $10^{-5}$  at 6 dB  $E_b/N_0$  for 600 bps rate for both AWGN and ARN with signal enhancement cases, and (ii) the BER performance for cases of AWGN and ARN with signal enhancement are similar.

## 7. CONCLUSIONS

The system architecture for high data rate VLF communication optimizes the performance based on the assumption of simplex communication. This allows tolerance of few seconds of algorithmic delay because of the one-way communication. The architecture adheres to the use of non-data aided techniques for carrier phase synchronization, symbol timing synchronization and LDPC frame synchronization which helps in maximizing the data throughput. This work required the development of novel techniques for iterative synchronization of carrier phase and symbol timing synchronization stages, and error variance based removal of symbol timing ambiguity. For each block, the promising alternatives were considered and simulated to decide on the best technique for the overall system. The BER performance analysis shows that the higher data rates are achievable with low probability of error under realistic atmospheric radio noise conditions.

## ACKNOWLEDGMENTS

This work was done as part of two projects from DEAL, Dehradun. The authors acknowledge the useful interactions with DEAL scientists during the course of this work. The contributions of Anindya Gupta, S.S. Lokesh, Hemlata Choudhary and Rinki Gupta of CARE IIT Delhi, in carrying out various simulation experiments is also acknowledged.

## REFERENCES

1. Pasupathy, S. Minimum shift keying: A spectrally efficient modulation. *IEEE Communications Magazine*, 1979, **17**(4), 14–22.
2. Mandayam, N. B. Wireless communication technologies. Lecture Notes, Advanced Topics in Communication Engineering, Rutgers University, 2002.
3. Murota, K. & Hirade, K. GMSK modulation for digital mobile radio telephony. *IEEE Trans. Communications*, 1981, **29**(7), 1044–1050.
4. Elnoubi, S.M. Analysis of GMSK with discriminator detection in mobile radio channels. *IEEE Trans. Vehicular Technol.*, 1986, **VT-35**(2), 71-76.
5. Report on electromagnetic compatibility of radio based mobile telecommunication systems. Appendix D, LINK Personal Communications Programme, University of Hull, UK, 1999.
6. Lui, G.L. & Tsai, K. Gaussian minimum shift keying precoding communication method. U.S. Patent 7,072,414 B1, 4 July, 2006.
7. Hwang, K.H. & Wickert, M. A. A soft output GMSK demodulator using A 4-Filter MLSE for small  $BT$  product. *Proc. IEEE ICC*, 2002, **5**, 2957–961.
8. Sanchez-Perez, R.; Pasupathy, S. & Casajus-Quiros, F.J. Envelope-aided viterbi receivers for GMSK signals with limiter-discriminator detection. *IEEE Trans. Communications*, 2004, **52**(10), 1733-746.
9. Yongacoglu, A. & Makrakis, D. Differential detection of GMSK using decision feedback. *IEEE Trans. Communications*, 1988, **36**(6), 641-49.
10. Tsai, K. & Lui, G.L. Coherent Viterbi and threshold demodulators for pulse-driven GMSK signals. *Proc. IEEE MILCOM*, 1999, **1**, 291-295.
11. Kaleh, G.K. Simple coherent receivers for partial response continuous phase modulation. *IEEE J. Selected Areas Communications*, 1989, **7**(9), 1427-436.
12. Kaleh, G.K. Differential detection via the Viterbi Algorithm for Offset Modulation and MSK-Type Signals, *IEEE Trans. Vehicular Technol.*, 1992, **41**(4), 401-06.
13. Laurent, P.A. Exact and approximate construction of digital phase modulations by superposition of amplitude modulated pulses, *IEEE Trans. Communications*, 1986, **34**, 150-160.
14. Hirade, K. & Murota, K. A study of modulation for digital mobile telephony. In the Proceedings of 29<sup>th</sup> IEEE Vehicular Technology Conference, 1979, **29**, 13-19.
15. Suzuki, H.; Yamao, Y. & Kikuchi, H. A single-chip MSK coherent demodulator for mobile radio transmission. *IEEE Trans. Vehicular Technol.*, 1985, **34**(4), 157-68.
16. Vassallo, E. & Visintin, M. Carrier phase synchronization for GMSK signals, *Int. J. Satell. Comm.*, 2002, **20**, 391-415.
17. Yik-Chung, Wu & Tung-Sang, Ng. Symbol timing recovery for GMSK modulation based on squaring algorithm, *IEEE Communications Letters*, 2001, **5**(5), 221-23.
18. Moon, T.K. Error correction coding: Mathematical methods and algorithms. Hoboken, NJ: John Wiley &

- Sons, Inc., 2006.
19. Gallager, R.G. Low density parity check codes. Cambridge, MA: MIT Press, 1963.
  20. MacKay, D.J.C. Good error-correcting codes based on very sparse matrices. *IEEE Trans. Infor. Theory*, 1999, **45**(2), 399-431.
  21. Berrou, C.; Glavieux, A. & Thitimajshima, P. Near Shannon limit error-correcting coding and decoding: Turbo Codes, *In the Proceedings of IEEE International Conference on Communications*, Geneva, Switzerland, 1993, 1064-070.
  22. Proakis, J. & Salehi, M. Digital communication. Ed 5. McGraw-Hill Education (Asia), 2008.
  23. Johnson, S.J. Introducing low density parity check codes. School of Electrical Engineering and Computer Science, University of Newcastle, Australia, Tech. Rept. SPM434.
  24. Felstrom, A.J. & Zigangirov, K.Sh. Time-varying periodic convolutional codes with low density parity check matrix, *IEEE Trans. Infor. Theory*, 1999, **45**(6), 2181-191.
  25. Sridharan, A. Design and analysis of LDPC convolutional codes. University of Notre Dame, USA, Feb. 2005. PhD Thesis.
  26. Pusane, A.E.; Zigangirov, K.Sh. & Costello, D.J. Construction of irregular LDPC convolutional codes with fast encoding. *In the IEEE International Conference on Communications*, Istanbul, Turkey, 2006, **3**, 1160-165.
  27. Costello, D.J.; Pusane, A.E.; Bates, S. & Zigangirov, K.Sh. A comparison between LDPC block and convolutional codes. *In the Workshop on Information Theory and its Application*, UCSD, La Jolla, CA, Feb. 2006.
  28. Richardson, T.J.; Shokrollahi, M.A. & Urbanke, R.L. Design of capacity-approaching irregular low-density parity-check codes. *IEEE Trans. Infor. Theory*, 2001, **47**(2), 619-637.
  29. Chung, S.Y.; Forney Jr., G.D.; Richardson, T.J. & Urbanke, R. On the design of low density parity check codes within 0.0045 db of the Shannon limit. *IEEE Comm. Lett.*, 2001, **5**(2), 58-60.
  30. Lee, D.; Kim, H.; Jones, C.R. & Villasenor, J.D. Pilotless frame synchronization for LDPC-coded transmission systems. *IEEE Trans. Signal Proces*, 2008, **56**(7), 2865-2874.
  31. Matzner, R. & Letsch, K. SNR estimation and blind equalization (deconvolution) using the kurtosis. *In the Workshop on Information Theory and Statistics*, 1994, 68.
  32. Harwood, J. Atmospheric radio noise at frequencies between 10 KC/s and 30 KC/s, *Institution Electrical Engineers*, 1958, Paper no. 2619 R, 293-300.
  33. Clarke, C. Atmospheric radio-noise studies based on amplitude-probability measurements at Slough, England, during the international geophysical year. *Institution Electrical Engineers*, 1962, Paper no. 3908 E, 393-404.
  34. Clarke, C.; Bradley, P.A. & Mortimer, D.E. Characteristics of atmospheric radio noise observed at Singapore, *Proc. IEE*, 1965, **112**(5), 849-60.
  35. Ibukun, O. Measurements of atmospheric noise levels. *Radio Electronic Engineer*, 1964, 405-15.
  36. Raab, F.H. Extraction of VLF-noise parameters. *Proc. MILCOM 92*, 1992, 1040-1045.
  37. Chrissan, D. & Fraser-Smith, A. A comparison of low-frequency radio noise amplitude probability distribution models. *Radio Science*, 2000, **35**(1), 195-208.
  38. Field Jr., E.C. & Lewinstein, M. Amplitude-probability distribution model for VLF/ELF atmospheric noise. *IEEE Trans. Comm.*, 1978, **COM-26**(1), 83-87.
  39. Nakai, T. & Ohba, H. On the graphical method of drawing APD's for atmospheric radio noise. *IEEE Trans. Electromagnetic Compatibility*, 1984, **26**(2), 71-78.
  40. Chrissan, D. Statistical analysis and modeling of low-frequency radio noise and improvement of low-frequency communications. Stanford Univ., Stanford, Calif., 1998. PhD Thesis.
  41. Chrissan, D. & Fraser-Smith, A. A clustering poisson model for characterizing the interarrival times of sferics, *Radio Science*, 2003, **38**(4), 1078.

### Contributors



**Dr Arun Kumar** received the BTech, MTech, and PhD in Electrical Engineering from the Indian Institute of Technology, Kanpur in 1988, 1990, and 1995 respectively. He is currently Professor and Head, Centre for Applied Research in Electronics, IIT Delhi. He has published 75 research papers and has supervised 40 funded R&D projects from Indian and foreign industries, as

well as various government organizations. He is a recipient of the Young Scientist award of the International Union of Radio Science. His current R&D work encompasses the topics of acoustics based target localization, voice personality transformation, text-to-speech synthesis in Indian languages, localization of acoustic transient signals, underwater acoustic communications, VLF communications, underwater acoustic signal processing, and design and realization of low power DSP hardware systems for remote unmanned operations.



**Professor R. Bahl** is a member of the faculty of CARE, IIT Delhi, where he heads the Signal Processing Group. He obtained his BTech (Electronics and Electrical Comm. Engg.) in 1974 from IIT Kharagpur, and his PhD (Electrical Engineering) IIT Delhi in 1982. His main area of work is in Underwater Electronics. He has delivered a number of projects, such as: a state-of-

the-art 3D imaging sonar SOBID, Programmable test signal generator for sonars, object visualisation using imaging sonars, CAD software package for high-resolution imaging sonars that simulates acoustic images of 3-D scenarios, MSK and GMSK modem design for VLF communication, Compact multiplexed multichannel SONAR system with proven superior performance in actual sea-trials: know how transferred to industry.